Ab initio calculation of chemisorption systems: H on Pd(001) and Pd(110)

D. Tománek and Z. Sun
Department of Physics and Astronomy and
Center for Fundamental Materials Research,
Michigan State University, East Lansing, Michigan 48824-1116

Steven G. Louie
Department of Physics, University of California, Berkeley, California 94720
and Materials and Chemical Sciences Division, Lawrence Berkeley Laboratory,
Berkeley, California 94720
(Received 4 September 1990)

We present an *ab initio* density-functional calculation of the interaction of hydrogen with the Pd(001) and Pd(110) surfaces and with bulk palladium. Our results for the H-Pd system are complemented by calculations for the H_2 molecule, the bulk, and the clean (001) and (110) surfaces of Pd. In the case of H in bulk Pd, we determine the equilibrium geometry and electronic structure and discuss the nature of the Pd—H bond. For the adsorption system H/Pd(001)and H/Pd(110), we determine the preferential adsorption sites, bond lengths, and vibration frequencies of the adsorbate. We relate H-induced softening of Pd-surface-phonon frequencies to a corresponding softening of Pd-Pd interactions in the bulk hydride phase.

I. INTRODUCTION

The interaction of hydrogen with transition metals is both fundamentally and technologically important.[1] The dissociative adsorption of molecular hydrogen at a metal surface and the subsequent surface and bulk diffusion of atomic hydrogen is a prototypical surface process. This is a well-suited model system for the study of the hydrogen-metal bond at different stages of the reaction. At least of equal importance is the microscopic understanding of the effect of hydrogen on the electronic and structural properties of the substrate metal. This effect, which has received less attention in the literature, manifests itself in H-induced surface relaxation and reconstruction, in phonon softening and decohesion, as well as significant changes of the electronic structure occurring both at the surface and in the bulk of the substrate metal.

The dissociation of H_2 at transition-metal surfaces is an important catalytic reaction that plays a key role in olefin hydrogenation, the Fischer-Tropsch process, and the ammonia synthesis.[2] The presence of hydrogen in bulk metals causes material embrittlement and cracking.[3] On the other hand, bulk metals are ideal media for safe storage of hydrogen in large quantities. More recently, substantial scientific effort has been made[4,5] to disprove reports of an apparent "cold-fusion" reaction[6] in deuterium-loaded transition metals.

We select the hydrogen-palladium system for our study, since it exhibits a rich variety of the above-described phenomena that causes this system to be of substantial technological interest. The physical properties of hydrogen on the Pd(001) surface have been investigated extensively by a variety of experimental methods such as thermal desorption spectroscopy (TDS),[7,8] work-function ($\Delta\phi$) measurements, and low-energy electron diffraction (LEED),[8] further by He scattering,[9] electron energy-loss spectroscopy,[10,11] and transmission channeling.[12] Hydrogen adsorption on this surface has been investigated previously by first-principles calculations[13] for different coverages. Equilibrium adsorption of hydrogen on the (110) surface of Pd has been investigated by LEED,[14] low energy ion scattering (LEIS),[15] He diffraction,[16] high-resolution electron-energy-loss spectroscopy (HREELS),[17,18] work-function and thermal desorption spectroscopy,[19,20] and by nuclear reaction analysis and Rutherford backscattering.[20] LEED studies indicate that at hydrogen coverages $\Theta > 1.5$, the Pd(110) surface exhibits a (1×2) reconstruction, probably of the missing-row-type,[21–23] even though the atomic positions in the substrate remain somewhat controversial.

The limited amount of theoretical information available is caused by the intrinsic difficulty to treat extended transition-metal surfaces owing to the coexistence of localized *d* electrons and delocalized *sp* electrons. Useful information about the Pd-H interaction can be obtained from accurate quantum-chemical calculations for very small Pd_nH_m clusters[24] or parametrized calculations for extended surfaces based on the embedded-atom method,[25,26] the embedded-cluster method[27], the effective medium method,[28] or the tight-binding formalism.[29] Only recently, however, have sufficiently powerful meth-

ods been introduced[30–34] that describe adsorbates on extended surfaces with adequate accuracy. We report here an *ab initio* calculation of the hydrogen-palladium interaction at the surface and in the bulk. Some of our results for H/Pd(001) and H in bulk Pd have been reported elsewher.[13,5] Our calculations for the interaction of H with the (001) and (110) surface and the bulk of Pd include equilibrium geometries, bond energies, vibration frequencies, and the electronic structure and the nature of the H—Pd bond. These studies are completed by corresponding calculations for the H_2 molecule, as well as hydrogen-free Pd(bulk), Pd(001), and Pd(110).

The paper is structured as follows. In Sec. II, we outline the application of the *ab initio* density-functional formalism to the H/Pd system. In Sec. III, we present our results for the pure constituents, namely hydrogen, bulk Pd, bulk PdH, and PdH_2 as well as H-free Pd(001) and Pd(110) surfaces. In Secs. IV and V, we describe the H-Pd interaction with Pd(001) and Pd(110), respectively. Finally, in Sec. VI, we summarize our results and present conclusions.

II. THEORY

We use the local-density approximation (LDA) (Ref. 35) to determine the total energy, the charge distribution, and the band structure of the Pd-H system in the ground state. The electron density $\rho(\mathbf{r})$ is obtained by solving self-consistently the Kohn-Sham equations[35]

$$\left(-\frac{\hbar^2}{2\,m}\nabla^2+V_{\rm ion}+V_{\rm H}+V_{\rm xc}\right)\psi_{n\mathbf{k}}=\varepsilon_{n\mathbf{k}}\psi_{n\mathbf{k}} \tag{1}$$

and

$$\rho(\mathbf{r})=\sum_{n\mathbf{k}}^{\rm occ}|\psi_{n\mathbf{k}}(\mathbf{r})|^2. \tag{2}$$

Here, $V_{\rm ion}$ is the potential due to the ion cores, V_H is the Hartree potential, and $V_{\rm xc}$ is the exchange-correlation potential for the charge density $\rho(\mathbf{r})$. In the pseudopotential formalism, we consider only the valence charge density, and replace $V_{\rm ion}$ by a first-principles pseudopotential that combines the nucleus and the core electrons into one entity.

Then, the total energy is given by

$$\begin{aligned}E_{\rm tot}=&\sum_{n\mathbf{k}}^{\rm occ}\varepsilon_{n\mathbf{k}}-\tfrac{1}{2}\int d\mathbf{r}\;V_H(\rho(\mathbf{r}))\rho(\mathbf{r})\\&-\int d\mathbf{r}\;V_{\rm xc}(\rho(\mathbf{r}))\rho(\mathbf{r})d\mathbf{r}\\&+\int d\mathbf{r}\;\varepsilon_{\rm xc}[\rho(\mathbf{r})]\rho(\mathbf{r})+E_{\text{ion-ion}},\end{aligned} \tag{3}$$

where $\varepsilon_{\rm xc}[\rho(\mathbf{r})]\rho(\mathbf{r})$ is the exchange-correlation energy density and $E_{\text{ion-ion}}$ describes the interaction between ion cores. In LDA, $\varepsilon_{\rm xc}[\rho(\mathbf{r})]$ is approximated by a local function $\varepsilon_{\rm hom}^{\rm xc}(\rho(\mathbf{r}))$.[35]

The use of local orbitals in the pseudopotential local orbital method[34] makes it computationally feasible to use high-energy cutoffs in the self-consistent calculation of Fourier components of the charge density and the potential. Our basis consists of local Gaussian-type orbitals of the form

$$f_{\alpha lm}(\mathbf{r})=A_{\alpha lm}e^{-\alpha r^2}K_{lm}(\theta,\phi), \tag{4}$$

which are localized on atomic sites and can be augmented by floating orbitals. $A_{\alpha lm}$ are normalization constants and K_{lm} are the Kubic harmonics $\{1,x,y,z,x^2,y^2,z^2,xy,yz,zx\}$ for l=0,1,2. We use norm-conserving ionic pseudopotentials of the Hamann-Schlüter-Chiang-type[36] and the Hedin-Lundqvist[37] form of the exchange-correlation potential in the local-density approximation.

Our criterion for the self-consistent solution of Kohn-Sham equations is a requirement that the maximum change in any Fourier component of the total potential $\delta V(\mathbf{G})$ between two successive iterations is smaller than 10^{-4} Ry. The Brillouin zone is sampled by a homogeneous mesh of $\mathbf{k}$ points that are generated using a special-point scheme.[38] Within the limits of the computational technique and the finite basis set, the typical precision of the total energy is of the order $<10^{-4}$ eV.

III. PURE CONSTITUENTS

A. Hydrogen

Pseudopotentials for isolated hydrogen atoms or molecules are introduced for the sake of convenience only. If the cutoff radius for the pseudopotential is small enough (in our calculation $r_c=0.35$ a.u.), the eigenvalues and eigenstates are insensitive to the singularity in the potential at the origin. Using the Hedin-Lundqvist form of the exchange-correlation potential, we find the total energy of the hydrogen pseudoatom to be −13.26 eV, taking into account the calculated spin-polarization energy of 1.04 eV.

For hydrogen in a crystal environment, we use a Gaussian basis consisting of s and p states with four radial decays each, i.e., 16 independent functions. The decay constants α, obtained by minimizing the total energy of hydrogen and fitting the ground-state wave function, are 0.20, 0.42, 0.68, and 1.36 in atomic units. For the calculation of H_2, an arrangement of supercells with the dimensions 9 a.u.×9 a.u.×11 a.u. has been chosen to minimize wave-function overlap between neighboring cells. We use a cutoff energy of 64 Ry for the Fourier components of the potential and charge density. In the ${}^1\Sigma_g^+$ ground state of the H_2 molecule, we obtain $r_e=0.78$ Å for the equilibrium distance (expt.[39] 0.74 Å) and $\omega_e=4100$ cm^{-1} for the vibration frequency (expt.[39] 4401 cm^{-1}). A dissociation energy[40] $D_e=4.71$ eV (expt.[39] $D_e=4.75$ eV) is obtained by comparing the total energy of H_2 to that of a supercell arrangement of hydrogen atoms (corrected by the spin-polarization energy).[41]

B. Palladium

Since electronic and structural properties of Pd have been studied previously,[42] we quote only those results that are relevant for a comparison with hydrogen compounds. We find the energy of the isolated Pd pseudoatom to be −796.414 eV, using the Hedin-Lundqvist form of the exchange-correlation potential. We consider s, p, and d valence orbitals with four radial Gaussian decays α each, i.e., 40 independent basis functions for each site. The palladium decays, which minimize the bulk total energy, are α = 0.27, 0.77, 2.18, and 6.20 in atomic units. Equilibrium properties of bulk fcc Pd are obtained by considering Fourier components of the potential and charge density up to a cutoff energy of 64 Ry. We sample the irreducible part of the bulk Brillouin zone by 47 **k** points. Our results for the calculated cohesive energy $E_{\rm coh}$ of bulk Pd as a function of the lattice constant a are shown in Fig. 1. The calculated equilibrium lattice constant a = 3.90 Å is in excellent agreement with the experimental value[43] of 3.89 Å. The bulk modulus of 2.15×10^{12} dyn/cm^2 agrees well with the experimental value[43] of 1.81×10^{12} dyn/cm^2. The calculated total energy at equilibrium of −799.79 eV corresponding to a Pd(bulk) cohesive energy of 3.37 eV (with respect to the isolated pseudoatom) underestimates the experimental value[43] of 3.89 eV. A possible reason for the low value of the Pd cohesive energy is an insufficient basis set. Actually, we do find that extending our basis set by floating orbitals at interstitial sites increases the value of the calculated cohesive energy by 0.2 eV, but does not affect energy differences that occur in calculations of elastic properties, etc. We also checked the convergency of our results with respect to the cutoff energy. Due to the smooth Pd pseudopotential that we use, Fourier compo-

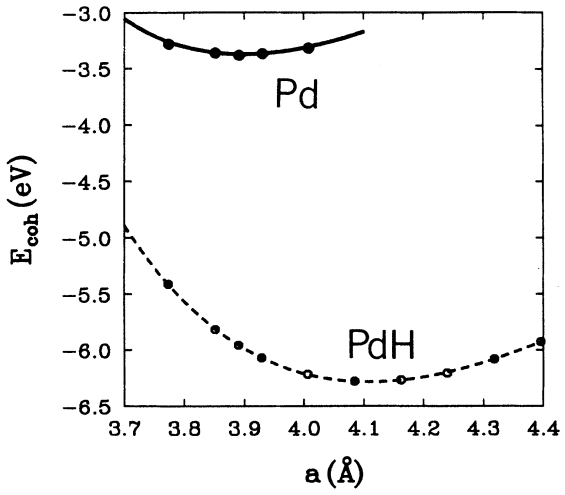

FIG. 1. Cohesive energy $E_{\rm coh}$ as a function of the lattice constant a for bulk Pd (solid line) and bulk PdH (dashed line).

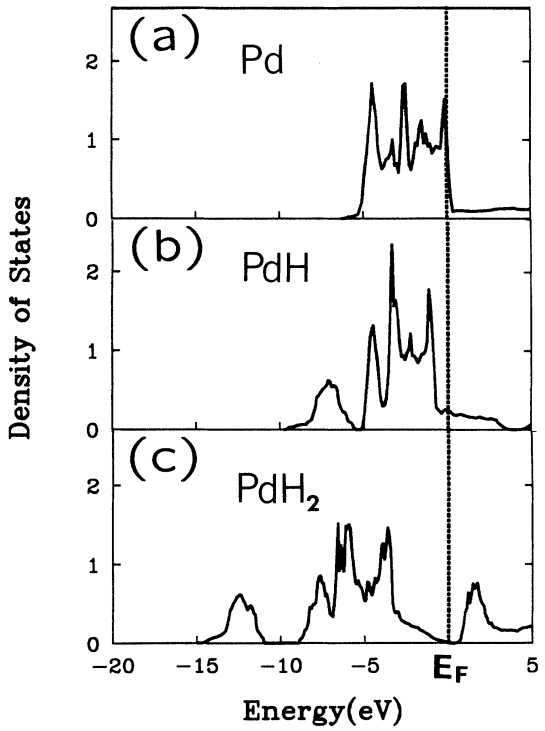

FIG. 2. Calculated electronic density of states $N(E)$ of (a) Pd, (b) PdH, and (c) PdH_2 ($d_{\rm H\text{-}H}$ = 0.74 Å).

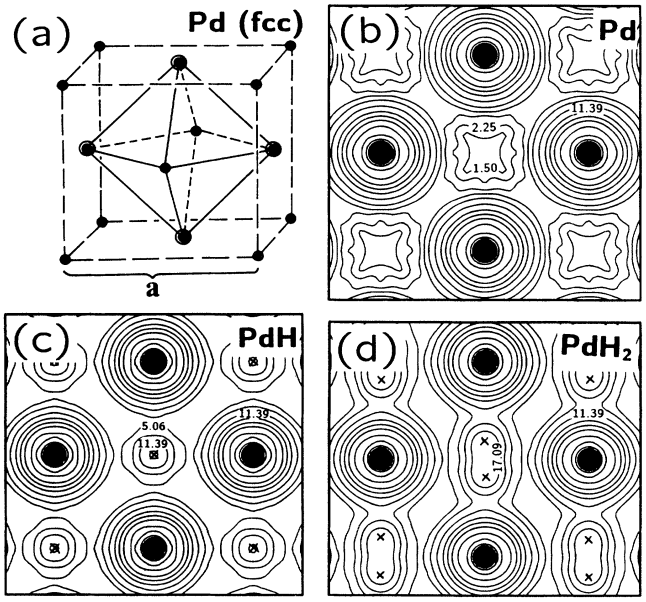

FIG. 3. (a) Conventional unit cell of Pd(fcc), with the octahedron cage shown by a solid line. Calculated charge density ρ(r) of (b) bulk Pd, (c) PdH, and (d) PdH_2 ($d_{\rm H\text{-}H}$ = 0.74 Å). All contour plots are shown in the (100) plane, which contains the four circled Pd atoms of the octahedron cage. The position of Pd atoms is marked by •; that of H atoms by ×. The charge density is in units of 10^{-2} e/a.u.^{3}; the ratio of two consecutive contours is $\rho(n+1)/\rho(n)$=1.5.

nents of the charge density die off rapidly and the total energies obtained with a 64- and 196-Ry cutoff differ by less than 0.1 eV.

The electronic structure of Pd is characterized by a nearly filled $4d$ band and a partially filled $5s$ band. The density of states $N(E)$ of Pd, presented in Fig. 2(a), shows the Fermi level near the top of the 5-eV-wide $4d$ band. The large value of $N(E_F)$ is responsible for very good conduction properties of this metal. A schematic drawing of the Pd structure, depicting the octahedral cage, is given in Fig. 3(a). The charge density of Pd in the (001) plane (containing four octahedral cage atoms) is shown in Fig. 3(b).

C. Palladium hydride and palladium dihydride

Palladium hydride PdH is a stable compound that forms spontaneously by exposing palladium metal to a hydrogen atmosphere. In this process, the palladium lattice retains the fcc structure, but the lattice constant is observed to increase by 6% due to hydrogen uptake in the high density phase.[44] H atoms occupy the octahedral interstitial sites in the Pd lattice [see Fig. 3(a)], which corresponds to the NaCl structure for the compound.

In an attempt to understand the equilibrium properties of Pd at various concentrations of hydrogen, we present results for both PdH and a hypothetical compound PdH_2. The latter results, interpreted for the chemically equivalent compound PdD_2,[5] have implications on the feasibility of the reported "cold-fusion" reaction in a Pd matrix.[6]

Basis functions for Pd and H have been discussed in the preceding subsections on the elements. In analogy to bulk Pd, we use an energy cutoff of 64 Ry in the Fourier expansion of the charge density and potentials in order to ensure complete convergence of the LDA spectrum and total energies. The LDA charge density and potentials have been obtained by sampling the Brillouin zone with a fine mesh of 1331 **k** points. Our total-energy calculation for PdH yields the equilibrium lattice constant $a = 4.1$ Å, which compares well with the experimental value[44] 4.12 Å. The calculated bulk modulus of 1.95×10^{12} dyn/cm^2 lies $\approx$10% below the value of bulk Pd, indicating H-induced softening.

We define the cohesive energy of PdH_n with respect to *isolated* atoms by

$$E_{\rm coh}(PdH_n) = E_{\rm total}(PdH_n) - E_{\rm total}(\text{Pd atom}) - nE_{\rm total}(\text{H atom}) \ . \quad (5)$$

For PdH, we find $E_{\rm coh}(\text{PdH}) = -6.28$ eV, which compares favorably with the experimental value[45] $E_{\rm coh}^{\rm expt}(\text{PdH}) = -6.65$ eV.

In order to obtain the equilibrium structure of PdH_2, we first study the interaction potential between two hydrogen atoms sharing the same octahedron cage.[5] A decrease of the hydrogen (or deuterium) bond length due to the metal matrix is likely to favor a "cold-fusion" reaction between deuterons. Such a bond-length reduction is conceivable in the case that H_2 aligns with its axis between the bottom and the top Pd atoms in the octahedron cage. Our results indicate that in this geometry, the intramolecular distance $d(H_2)$ is *expanded* to 0.94 Å in the Pd lattice. This makes the "cold" nuclear fusion in Pd even less probable than in the D_2 gas phase. For this equilibrium H_2 bond length, we find the cohesive energy of PdH_2 to be $E_{\rm coh}(PdH_2) = -6.78$ eV.

Our results have been confirmed by independent calculations of H_2/Pd(bulk), which also consider different molecular orientations.[46] These calculations predict a spontaneous reorientation of the H_2 molecule from the [001] to the [111] direction, accompanied by a further increase of the bond length.

The stability of palladium hydride compounds can be investigated best by comparing formation energies of PdH_n (starting from *bulk* palladium and *molecular* hydrogen), which is given by

$$E_{\rm form}(PdH_n) = E_{\rm total}(PdH_n) - E_{\rm total}(\text{Pd bulk}) - \frac{n}{2}E_{\rm total}(H_2 \text{ molecule}). \quad (6)$$

This definition yields $E_{\rm form}(\text{PdH}) = -0.53$ eV and $E_{\rm form}(PdH_2) = +1.34$ eV indicating a compound forming tendency of PdH and structural instability of PdH_2, again in agreement with experiment.

Cohesive properties of the Pd-H systems and the origin of the large distance between hydrogen atoms in bulk Pd can be best understood by inspecting the electronic density of states and the corresponding charge density. In Fig. 2 we compare the total density of states of PdH_2 to that of PdH (at the same volume) and to bulk Pd at its equilibrium volume. In agreement with previous calculations for PdH in the bulk phase[47] and for the surface adsorption[13] of H/Pd(001), we find that the binding between H and Pd is predominantly covalent, giving rise to a bonding split-off state at ≈ -13 eV (with respect to E_F) in PdH_2 [Fig. 2(b)] and at ≈ -8 eV in PdH [Fig. 2(c)]. To a lesser extent, hybridization with hydrogen also modifies the $4d$ density of states of Pd. With increasing H concentration, the $4d$ band is being pulled below the Fermi level and filled, decreasing the contribution of d electrons in bonding. In the extreme case of PdH_2, Fig. 2(c) suggests a transition to a semimetal.

In Fig. 3 we compare total charge densities of PdH_2, PdH, and bulk Pd. Due to the large lattice constant of Pd, the H atom and H_2 molecule fit easily into the Pd octahedral cage [Figs. 3(c) and 3(d)] and fill the low charge-density region inside [Fig. 3(b)]. Even at a H-H distance of 0.74 Å, the separation between H and Pd atoms is close to 1.7 Å, which is a typical Pd—H bond length. Due to the small size of the H atom in the octahedral cage, the interaction potential with the surrounding Pd matrix is very soft and gives rise to very low H vibration frequencies. From the charge-density difference we conclude that there is a small net charge transfer from Pd to H ($\approx 0.2\ e$ near the equilibrium distance which is typical for all Pd-H systems). From the population anal-

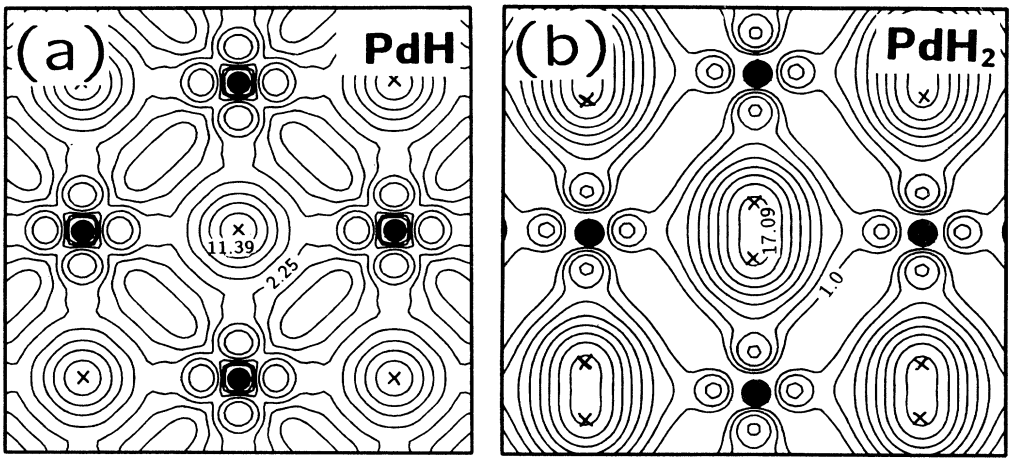

FIG. 4. Charge density $\rho(\mathbf{r})$ corresponding to hydrogen-induced split-off states [at $E \approx -8$ eV in Fig. 2(b) and $E \approx -13$ eV in Fig. 2(c)] of (a) PdH and (b) PdH_2 ($d_{H-H} = 0.74$ Å). Both contour plots are shown in the (100) plane, which contains the four circled Pd atoms in Fig. 3(a). The position of Pd atoms is marked by •; that of H atoms by ×. The charge density is in units of 10^{-2} e/a.u.^{3}; the ratio of two consecutive contours is $\rho(n+1)/\rho(n)$=1.5.

ysis we conclude that this charge originates mainly from the Pd 5s band.

The inspection of the charge density associated with H-induced split-off states in PdH and PdH_2, shown in Figs. 4(a) and 4(b), shows that these states are predominantly of H 1s–Pd 4d character, and are centered in the middle of the octahedron cage. The large binding energy of these states, mainly due to the attractive H^+ potential, increases with increasing hydrogen concentration, which stabilizes these compounds. This effect is counteracted by the contribution of the H-induced antibonding levels. These levels, nearly empty at low hydrogen concentrations, are pulled to higher binding energies and populated, which leads to a destabilization of Pd-H compounds at increasing hydrogen concentrations.

D. Clean Pd(001) and Pd(110) surfaces

Atomic arrangement in the Pd(001) and Pd(110) surfaces is shown in Figs. 5(a) and 5(d). In our calculation, these surfaces are modeled by slabs of finite thickness. Due to the small value of the Thomas-Fermi screening length in metals, three to five metal layers are sufficient to decouple the two sides of the slab. We use a repeated slab geometry and separate metal slabs by a "vacuum slab" of sufficient thickness (typically ≈10 Å) in order to avoid the surface charge density and potential being affected by neighboring slabs.

The surface energy can be derived from the total energy of the bulk and of an n-layer slab using

$$E_s^0 = \tfrac{1}{2}[E_{\text{total}}(\text{slab}) - nE_{\text{total}}(\text{bulk})]. \quad (7)$$

In our calculation, we used a cutoff energy of 64 Ry for the Fourier components of the charge density and potential. In order to represent the charge decay in the vacuum region accurately, we augmented Pd-based basis functions (given in the section on bulk Pd) by floating orbitals in the vacuum region. The good result for the Pd(001) work function $\phi = 5.25$ eV ($\phi = 5.22$ eV has been observed in an equilibrated Pd film[48]) suggests that the surface dipole moment and charge density have been determined with adequate accuracy. Our values for the surface energies of Pd(001) and Pd(110), based on three-layer Pd slab calculations, are $E_s^0(001) = 0.49$ eV/atom and $E_s^0(110) = 1.80$ eV/atom. For computational reasons, we expect the true physical value of the Pd(110) surface energy to be smaller than our calculated value suggests.[49] Nevertheless, our LDA results are consistent with an intuitive argument suggesting that the surface energy of the more open (110) surface should be larger than that of the close-packed (001) surface.

Since no precise experimental data exist for the surface energy of these single-crystal surfaces, we obtain a rough estimate using the second-moment approximation in the tight-binding technique,[50]

$$E_s^0 \approx E_{\text{coh}}(\text{bulk}) \sum_i [1 - (Z_i/Z_{\text{bulk}})^{1/2}]. \quad (8)$$

Here, the summation is over all inequivalent surface sites i, and Z_i is the corresponding coordination number. Based on this formula, and using the experimental value of the bulk cohesive energy[43] $E_{\text{coh}} = 3.89$ eV, the surface energies of the (001) and (110) surfaces of Pd, based on Eq. (8), are $E_s^0(001) \approx 0.7$ eV/atom and $E_s^0(110) \approx 1.1$ eV/atom. Our LDA values are consistent with the tight-binding estimate, and also lie close to estimates obtained by Miedema[51] for the surface energy of close-packed surfaces $E_s^0 \approx 2.1$ J m^{-2} ≈ 1.0 eV/atom.

Differences in the surface energy between these two surfaces are reflected in the surface (or slab-averaged) electronic density of states (DOS) $N(E)$, shown in Figs. 5(b) and 5(e). These *surface* DOS's can be thought of as a weighted average of the local DOS of the topmost and second layer of a Pd crystal terminated with a (001) or (110) surface. In agreement with the intuition, the apparent width (or the second moment) of $N(E)$ is smaller for the more open (110) surface than the (001) surface. Due to the lower coordination of surface atoms, both surfaces show a narrower surface $4d$ band than bulk Pd (see Fig. 2). Naturally, the *total* DOS of semi-infinite samples equals the bulk DOS due to the overwhelming number of bulk atoms.

The total charge density $\rho(\mathbf{r})$ of the Pd(001) and (110) surfaces, shown in Figs. 5(c) and 5(f), lies very close to a charge density obtained from the superposition of atomic charge densities. We conclude that the charge transfer, the presence of directional bonding, and the crystal field play only a minor role in the charge distribution.

IV. HYDROGEN ADSORPTION ON Pd(001)

The adsorption energy $E_{\rm ad}$ reflects the strength of the adsorption bond. The value per adsorbed atom can be obtained from the total-energy difference between the adsorption system, the clean surface, and the free adsorbate. For atomic hydrogen adsorbed on Pd(001), we obtain

$$E_{\rm ad}(\Theta) = \frac{1}{\Theta}\{E_{\rm total}[{\rm H/Pd(001)}] - E_{\rm total}[{\rm Pd(001)}]\} - E_{\rm total}({\rm H\ atom})\ , \tag{9}$$

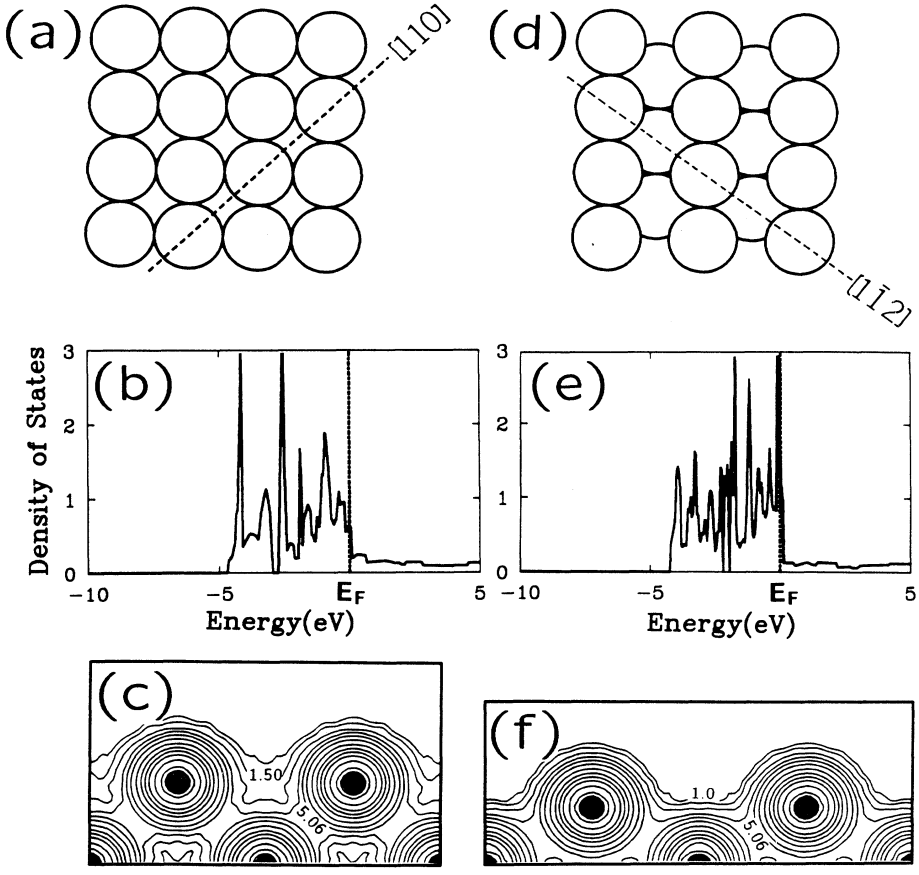

FIG. 5. Top view of the atomic arrangement, surface (slab-averaged) electronic density of states $N(E)$ and charge density $\rho(\mathbf{r})$ of the Pd(001) surface [(a)–(c)] and the Pd(110) surface [(d)–(f)]. The contour plots of $\rho(\mathbf{r})$ are shown in the (1$\bar{1}$0) plane (which contains the [110] direction) for the (001) surface and in the ($\bar{1}$11) plane (which contains the [1$\bar{1}$2] direction) for the (110) surface. The position of Pd atoms is marked by •. The charge density is in units of 10^{-2} e/a.u.^{3}; the ratio of two consecutive contours is $\rho(n+1)/\rho(n)$=1.5.

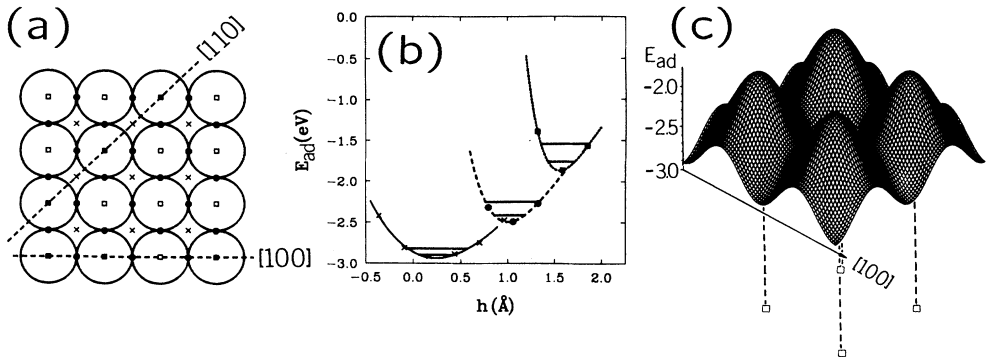

FIG. 6. (a) Schematic top view of Pd(001) and the assignment of adsorption sites: hollow (×), bridge (•), and on top (□). (b) H adsorption energy E_{ad} on Pd(001) as a function of the adsorption height h. The lowest two vibration levels are indicated in the potential wells. (c) Potential-energy surface E_{ad} for H/Pd(001) as a function of the hydrogen position in the surface plane, presented as a $3d$ plot. The position of Pd atoms is indicated by □ in (c).

where the coverage Θ denotes the ratio between the numbers of adsorbed and topmost layer substrate atoms. In our calculation, we consider hydrogen to be adsorbed to both sides of the slab representing Pd(001). Then,

$$E_{ad}(\Theta) = \frac{1}{2\Theta}\{E_{total}[\text{H/Pd(001) slab}] - E_{total}[\text{Pd(001) slab}]\} - E_{total}(\text{H atom}) \ . \quad (10)$$

A schematic view of the Pd(001) surface and the high-symmetry adsorption sites is presented in Fig. 6(a) and the H-Pd interaction potentials in these sites are shown in Fig. 6(b). Table I summarizes the calculated equilibrium values of the adsorption bond energy E_{ad}, the equilibrium height (with respect to the topmost Pd layer) h_0, and the harmonic vibration frequency ω for these sites.

A comparison of the above adsorption energy results, obtained for a three-layer Pd slab, to corresponding five-layer Pd slab results, showed that the differences lie within the experimental error of ± 0.02 eV. Similar agreement was obtained for the vibration frequencies. Basis functions for Pd and H have been discussed in the preceding subsections on the elements. In analogy to bulk Pd, we used an energy cutoff of 64 Ry in the Fourier expansion of the charge density and potentials in order to ensure complete convergence of the LDA spectrum and total energies. The completeness of our basis set and the **k**-point sampling of the Brillouin zone have been tested by investigating the dependence of the total energy on the number of basis functions and **k** points.

In order to obtain accurate values for the heat of adsorption with a localized basis, we extended the basis set by including additional floating orbitals at sites not occupied by atoms. The basis set used for the calculation of hydrogen in hollow sites also included orbitals at all bridge and on-top sites. The total energy for hydrogen in bridge or on-top sites has been obtained by keeping essentially the same basis and "switching" the hydrogen ionic potential to the respective sites. For the adsorbate-free Pd slab, all basis sites at adsorbate positions were kept but carried zero potential. Using this procedure, we were able to treat various geometries on equal footing in the orbital space and to obtain accurate energy differences between the adsorption sites.

Since our calculations are for ordered monolayers, adsorption energies contain adsorbate-adsorbate interactions to all orders and are useful for the calculation of adsorption phase diagrams.[52] As in all LDA calculations,

TABLE I. Calculated and observed values of the adsorption bond energy E_{ad}, adsorption height h_0, and vibration frequency ω for H on Pd(001).

Adsorption site	Coverage Θ	E_{ad} (eV) Calc.	E_{ad} (eV) Expt.	h_0 (Å) Calc.	h_0 (Å) Expt.	ω (meV) Calc.	ω (meV) Expt.
Hollow	1.0	−2.92	−2.77[a]	0.24	0.30 ± 0.05[b]	77	64[c]
Bridge	2.0	−2.50		1.00		165	
On top	1.0	−1.86		1.56		217	

[a] Reference 8.
[b] Reference 12.
[c] Reference 11.

we find our adsorption system slightly overbound when comparing to observed adsorption energies. Previous calculations indicate that this overbinding does not significantly affect energy differences between different adsorption sites. In Fig. 6(c), we show a $3d$ view of the potential energy $E_{\rm ad}$ for H along the Pd(001) surface,[53] which is useful when discussing the surface diffusion of hydrogen.

When making a comparison with the experiment, the value of $E_{\rm ad}$ must also be corrected to account for the zero-point-motion of the hydrogen atom in the potential well. Considering only vibrations perpendicular to the surface, and using the calculated vibration frequencies ω given in Table I, we find the zero-point-motion corrected values of $E_{\rm ad}$ to be -2.88 eV in the hollow site, -2.42 eV in the bridge site, and -1.75 eV in the on-top site.

Adsorption energies are related to the measured[8] isosteric heat of adsorption $H_{\rm ad}$ and the hydrogen dissociation energy $D_e(H_2)$ by

$$H_{\rm ad}(H_2) = -[2E_{\rm ad}(H) + D_e(H_2)] \ . \tag{11}$$

Using our calculated value $D_e(H_2) = 4.71$ eV, we obtain $H_{\rm ad} = 1.13$ eV for the hollow site, 0.29 eV for the bridge site, and -0.99 eV for the on-top site. Clearly, hydrogen will only adsorb dissociatively if the net energy gain $H_{\rm ad} > 0$. This is the case for the hollow and the bridge sites; hydrogen is not expected to occupy the on-top site.

For adsorbate-covered surfaces, we also define a modified surface energy (per surface Pd atom) by

$$E_s(\Theta) = \tfrac{1}{2}\{E_{\rm total}[{\rm H/Pd(001)\ slab}] - nE_{\rm total}({\rm Pd\ bulk})\} - \tfrac{1}{2}\Theta\ E_{\rm total}(H_2\ {\rm molecule}) \ . \tag{12}$$

Here, n is the number of Pd layers in a slab and the total energy of the slab $E_{\rm total}$[H/Pd(001) slab] is normalized to one Pd atom per layer. Using Eqs. (7), (10), and (11), we can express $E_s(\Theta)$ as

$$\begin{aligned} E_s(\Theta) &= E_s^0 + \tfrac{1}{2}\Theta[2E_{\rm ad}(\Theta) + D_e(H_2)] \\ &= E_s^0 - \tfrac{1}{2}\Theta H_{\rm ad}(H_2). \end{aligned} \tag{13}$$

In the case of a clean surface, $E_s(\Theta = 0)$ corresponds to Eq. (7). Our values for the heats of adsorption suggest that hollow- and bridge-site hydrogen stabilizes the Pd(001) surface by lowering the surface energy. Hydrogen in the (energetically) unstable on-top site would increase the surface energy.

Our results for the adsorption energies, summarized in Table I, establish that at low coverages, $\Theta < 1$, hydrogen occupies preferentially the hollow sites. This is also supported by the agreement between the calculated and measured adsorption heights[12] and vibration frequencies.[11]

In the coverage range $\Theta > 1$, the additional hydrogen atoms occupy new adsorption sites. As mentioned above, the on-top sites can be ruled out for this purpose. A simultaneous occupation of neighboring fourfold hollow and bridge sites is unlikely because of strong repulsive interactions between neighboring adatoms.[54,28] This is also confirmed by our calculation for a simultaneous occupation of hollow and bridge sites on Pd(001), which yields $E_{\rm ad} = -1.45$ eV at $\Theta = 3$, corresponding to a much weaker bond than in the on-top site.

From the total-energy balance for $\Theta > 1$, we find that bridge-bonded hydrogen (at a *local* coverage $\Theta = 2$) is unstable with respect to hydrogen desorption and occupation of hollow sites. This energy balance is expected to be more favorable for the bridge sites in cases of a *local* coverage well below $\Theta = 2$. We thus conclude that at coverages $\Theta > 1$, additional hydrogen atoms are likely to occupy bridge sites at a local coverage $1 < \Theta < 2$, or, more likely, will diffuse into the bulk. As mentioned in Sec. III C, the net energy gain for the latter process is 0.53 eV per H atom.

The calculated small value of the hydrogen adsorption height $h_0 = 0.24$ Å given in Table I for the hollow site is also in very good agreement with the experimental result[12] of $h_0 = 0.30 \pm 0.05$ Å for the $p(1 \times 1)$ phase of D on Pd. It should be noted that this adsorption geometry is very close to the octahedral absorption site of H in bulk Pd (see Fig. 3). The low value of h_0 results from the large Pd-H nearest-neighbor distance, which exceeds the sum of the Pd and H atomic radii. This is also the physical origin of the soft H-Pd interaction potential as a function of h near the equilibrium, as shown in Fig. 6(b), which results in a very low vibration frequency ω perpendicular to the surface. Our calculated value ω=77 meV agrees well with the observed[11] frequency ω=64 meV for Pd(001) and is also close to the bulk value ω=68.5 meV which has been reported[55] for the octahedral-site H in bulk PdH. The H-Pd interaction potential is very anharmonic and shows a sharp increase for low values of h due to an increased charge-density overlap between the hydrogen and second-layer Pd atoms. Similar results for the hollow-site hydrogen on Pd(001) have previously been obtained from an effective medium calculation,[28] which characterizes the adsorption system by a few parameters. From our calculation, we find that the Pd host electron density at h_0 varies by $< 20\%$ between the different adsorption sites. This establishes the limits of validity of the effective medium theory,[28] which averages out covalent effects in cohesion.[56] Our equilibrium adsorption geometries are also consistent with a H—Pd bond length of 1.6–1.7 Å in the bridge and on-top sites, which is equal to the sum of the atomic radii of Pd and H.

The effect of potential anharmonicity on the vibration frequency ω has been considered by expanding the lowest vibrational eigenstates of a general potential $E_{\rm ad}(h)$ in terms of the eigenstates of a linear harmonic oscillator (LHO). Up to nine LHO states have been used in the expansion and ω was determined from the difference of the two lowest vibrational levels. The two lowest vibrational levels are shown in Fig. 6(b) together with $E_{\rm ad}(h)$. In the hollow site, this procedure yielded a vibration frequency that differed by $\approx$8 meV from the harmonic frequency $\omega = 77$ meV. Our calculation of hydrogen vibration frequencies, however, considered only H displacements perpendicular to the surface at the high-symmetry sites. A coupling to vibration modes parallel to the surface is ex-

pected to reduce the lowest vibration frequency and bring it to closer agreement with the observed value[11].

As seen in Fig. 6(b), the hydrogen adsorption bond strength decreases in the sequence hollow → bridge → on-top site. In order to understand this trend, we show in Figs. 7(a)–7(c) the surface (slab-averaged) surface density of states $N(E)$ for the different adsorption sites. A comparison with the hydrogen-free Pd(001) surface density of states, given in Fig. 5(b), shows that the most prominent feature is a hydrogen-induced split-off state below the Pd 4*d* band, in close analogy with bulk Pd and PdH (see Fig. 2). The simple argument that strong adsorption bonds result from large adsorbate-substrate hybridization in highly coordinated sites is supported by comparing the energy difference $\delta\epsilon$ between the bottom of the Pd band and the split-off H-Pd bonding state. This quantity reflects the hybridization between palladium and hydrogen. Inspecting the densities of states, we find no split-off states for the on-top adsorption site, $\delta\varepsilon \approx 0.3$ eV for the bridge site, and $\delta\varepsilon \approx 1.1$ eV for the hollow site. Of course, we observe a decrease of $\delta\varepsilon$ with increasing H-Pd distance. The shallow potential $E_{\rm ad}(h)$ for hollow-site hydrogen results from a very slow variation in the adsorbate -substrate hybridization as a function of h, and is reflected in relatively small changes of $\delta\varepsilon$.

In Figs. 7(d)–7(f) we present the total charge density of the H/Pd(001) system for the different adsorption sites and h_0. The changing environment of the hydrogen atoms in the different adsorption sites modifies not only the depth, but also the shape of the H-Pd interaction potential, as shown in Fig. 6(b). The charge density for hollow-site hydrogen, shown in Fig. 7(d), exhibits a very small corrugation, which has been observed by He diffraction.[9] With decreasing coordination number, $E_{\rm ad}(h)$ resembles more a pairwise interaction potential that gives rise to an increasing vibration frequency ω.

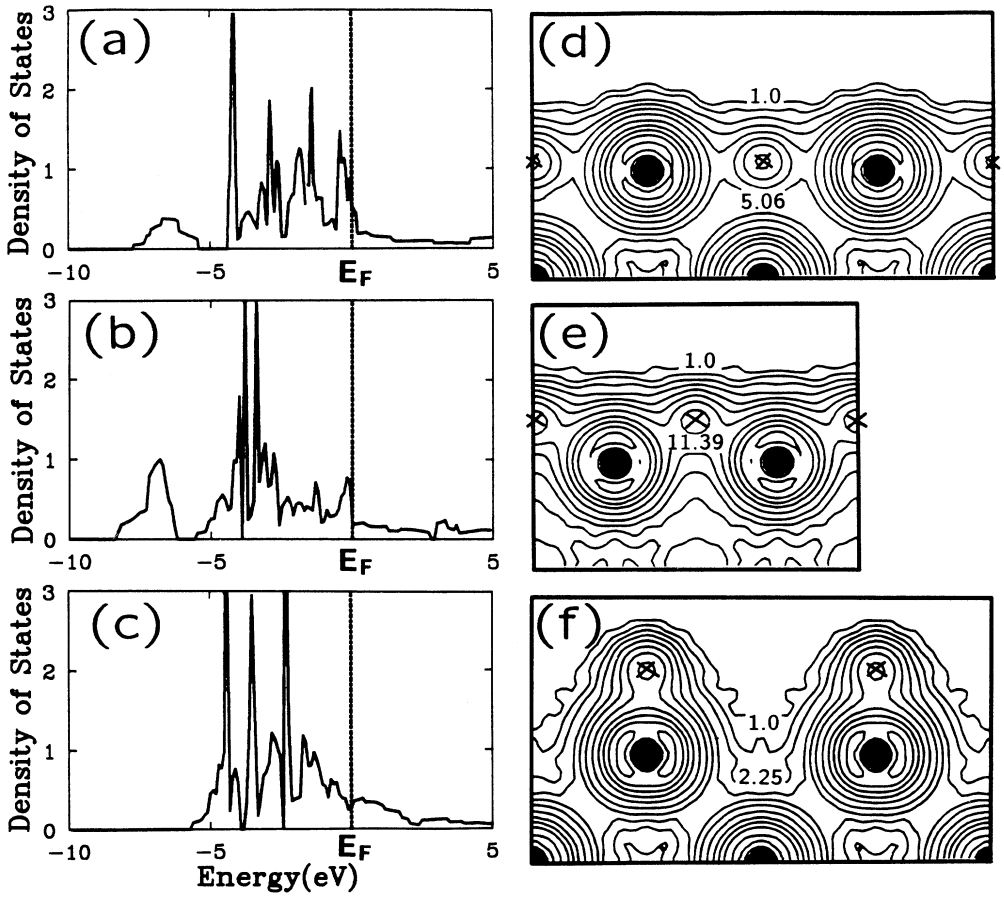

FIG. 7. Surface (slab-averaged) electronic density of states $N(E)$ for H/Pd(001) in the hollow (a), bridge (b), and on-top site (c). Charge density $\rho(\mathbf{r})$ for H/Pd(001) in the hollow (d), bridge (e), and on-top site (f), shown in the $(1\bar{1}0)$ plane (which contains the [110] direction). The position of Pd atoms is marked by • and that of H atoms by ×. The charge density is in units of 10^{-2} e/a.u.^{3}; the ratio of two consecutive contours is $\rho(n+1)/\rho(n)$=1.5.

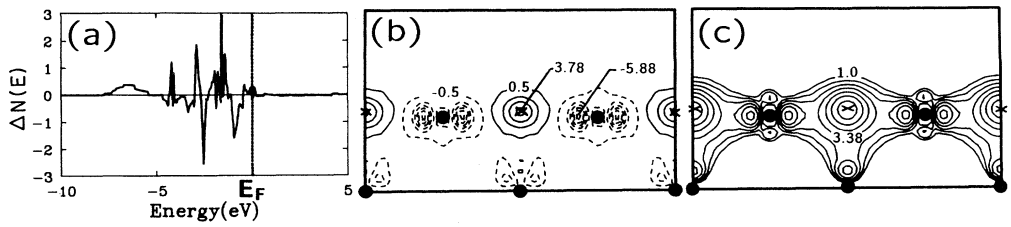

FIG. 8. (a) Difference density of states $\Delta N(E)$, (b) difference charge density $\Delta\rho(\mathbf{r})$, and (c) charge density associated with the H-induced split-off state [at $E \approx -7$ eV in Fig. 7(a)] for H/Pd(001) in the hollow site. The position of Pd atoms is marked by • and that of H atoms by ×. The charge density is in units of 10^{-2} e/a.u.^{3}. In (b), the consecutive contours are separated by 10^{-2} e/a.u.^{3}, and in (c) the ratio of two consecutive contours is $\rho(n+1)/\rho(n)$=1.5.

The work function depends very sensitively on the surface charge distribution, which establishes the surface dipole. Our calculated work function for the hollow site ($\Theta = 1$) $\phi = 5.53$ eV has increased by 0.3 eV with respect to the hydrogen-free surface; a similar increase of 0.11 eV has been determined experimentally for this surface.[8]

To establish the nature of the hydrogen-palladium surface bond, we determine the difference density of states $\Delta N(E) \equiv N_{\mathrm{H/Pd(001)}}(E) - N_{\mathrm{Pd(001)}}(E)$ and the charge-density difference $\Delta\rho \equiv \rho_{\mathrm{H/Pd(001)}} - \rho_{\mathrm{Pd(001)}} - \rho_{\mathrm{H}}$ for the hollow-site hydrogen. An inspection of the difference density of states for the hollow site, given in Fig. 8(a), shows that the main effect of hydrogen is to induce a split-off state below the bulk Pd band, and—to a lesser extent—modify the Pd $4d$ band. An analysis of the charge-density difference, given in Fig. 8(b), shows a charge transfer of ≈0.2 electrons towards hydrogen, stemming mainly from Pd atoms in the topmost layer. The nature of the H-Pd bonding mechanism can be seen from the charge density associated with the H-Pd split-off state at ≈ 7 eV below the Fermi level in Fig. 8(a), shown in Fig. 8(c). The covalent bonds result mainly from the hybridization of H $1s$ and Pd $4d$ states and are mostly localized in the topmost surface layer. These states are very close in character to the H-induced split-off states in bulk PdH and PdH_2, which are analyzed in Fig. 4.

V. HYDROGEN ADSORPTION ON Pd(110)

In this section, we will discuss hydrogen adsorption on Pd(110) along the lines of H/Pd(001). When presenting numerical results, we will use obvious modifications of the expressions for the adsorption bond energy E_{ad} and surface energy $E_s(\Theta)$ given in Eqs. (9), (10) and (12).

As illustrated in Figs. 5(d) and 9(a), Pd(110) is a very open surface. This is the origin of the large surface energy value discussed in Sec. III D, but also raises the question of surface relaxations. Figure 9(a) gives a side view of a relaxed Pd(110) surface. The vertical relaxation, indicated in Fig. 9(a), is defined by $\Delta d_{12} \equiv (d_{12}/d_{12}^0 - 1)$,

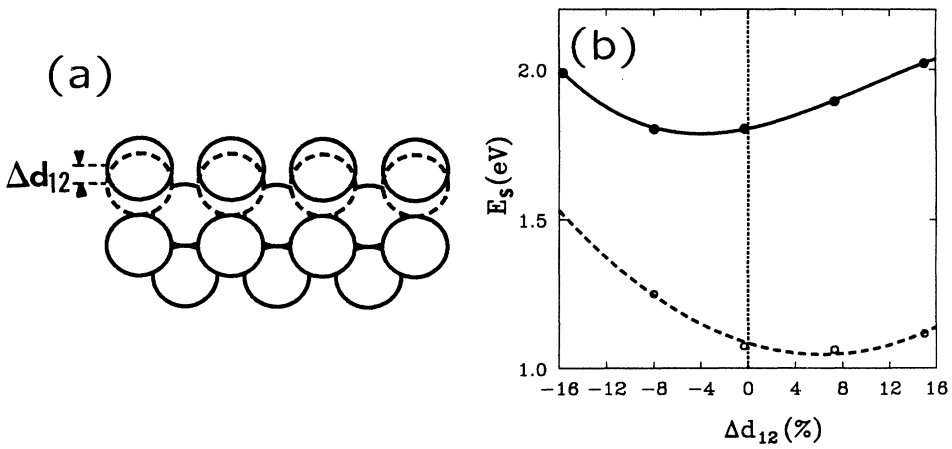

FIG. 9. (a) Schematic side view of the Pd(110) surface. (b) Surface energy as a function of the vertical relaxation Δd_{12} of the first interlayer spacing in Pd(110). The solid line corresponds to a clean Pd(110) surface and the dashed line to a H-covered (Θ=1, hollow site) surface.

where $d_{12}^0 = 1.38$ Å is the bulk interlayer spacing. Our results for the surface energy of clean Pd(110), given by the solid line in Fig. 9(b), indicate a contraction $d_{12} = -4\%$ of the topmost layer spacing. In view of the fact that we did not consider multilayer relaxations, this value agrees well with the LEED result[14] $d_{12} = -5.1\%$ and with the general trend observed and calculated for surfaces of late transition metals.[14,57] It is conceivable that a separate consideration of multilayer relaxations could enhance Δd_{12} (by reducing the repulsion between the topmost and the third layer).[58]

In analogy to H/Pd(001), H adsorption lowers the surface energy by saturating Pd dangling bonds and consequently reverses the contraction. This is shown by the dashed line in Fig. 9(b), which corresponds to a hydrogen-covered surface. In our calculation, we assumed the H atoms to be adsorbed in the hollow site (see Fig. 10) and kept the distance between hydrogen and second-layer Pd atoms fixed. For a monolayer coverage of hydrogen, our results indicate a 6% surface expansion. This expansion is reminiscent of the value observed in bulk Pd upon hydrogen uptake and reflects similarities in the Pd—H bond.

As shown in Fig. 9(b), the Pd-Pd interplane interaction potential has a large anharmonicity, which has also been observed on the chemically similar Ni(110) surface.[59] The interplane force constant $c = 12.3$ eV/Å^2 at the Pd(110) surface is somewhat smaller than the bulk force constant $c = 15.4$ eV/Å^2 corresponding to a compression along the [110] direction. Hydrogen adsorption on Pd(110) lowers the interplane force constant to $c = 10.3$ eV/Å^2. A similar hydrogen-induced softening can be observed in the bulk (see Fig. 1), which corresponds to a decrease of the Pd bulk modulus in the hydride phase.

A schematic top view of the Pd(110) surface and the high-symmetry adsorption sites is presented in Fig. 10(a) and the H-Pd interaction potentials in these sites are shown in Fig. 10(b). All calculations have been performed in an analogous way to the Pd(001) surface described in the preceding section, for five-layer slabs consisting of three palladium layers and two hydrogen layers. Table II summarizes the calculated equilibrium values of the adsorption bond energy $E_{\rm ad}$, the equilibrium height (with respect to the topmost Pd layer) h_0, and the harmonic vibration frequency ω for these sites. A $3d$ view of the potential energy $E_{\rm ad}$ for H along the Pd(110) surface[53] is shown in Fig. 10(c).

When making comparison with the experiment, the value of $E_{\rm ad}$ has also to be corrected to account for the zero-point-motion of the hydrogen atom in the potential well. Considering only vibrations perpendicular to the surface, and using the calculated vibration frequencies ω given in Table II, we find the zero-point-motion corrected values of $E_{\rm ad}$ to be -3.38 eV in the long-bridge site, -2.98 eV in the hollow site, -3.00 eV in the short-bridge site, and -2.17 eV in the on-top site. Due to numerical difficulties similar to the calculation of the Pd(110) surface energy, these calculated values of $E_{\rm ad}$ probably exaggerate the strength of the adsorption bond.[49]

Using our calculated value $D_e(H_2) = 4.71$ eV, we obtain $H_{\rm ad} = 2.11$ eV in the long-bridge site, 1.43 eV in the hollow site, 1.39 eV in the short-bridge site, and -0.11 eV in the on-top site. Clearly, hydrogen will only adsorb dissociatively if the net energy gain $H_{\rm ad} > 0$. This is the case for the long-bridge, hollow, and short-bridge sites. Similar to the Pd(001) surface, hydrogen is not expected to occupy the on-top site.

Using Eq. (13) and these values for the heats of adsorption, we can determine the surface energy of hydrogen-covered Pd(110). Our results suggest that hydrogen in long-bridge, hollow, and short-bridge sites stabilizes the Pd(110) surface by lowering the surface energy. Hydro-

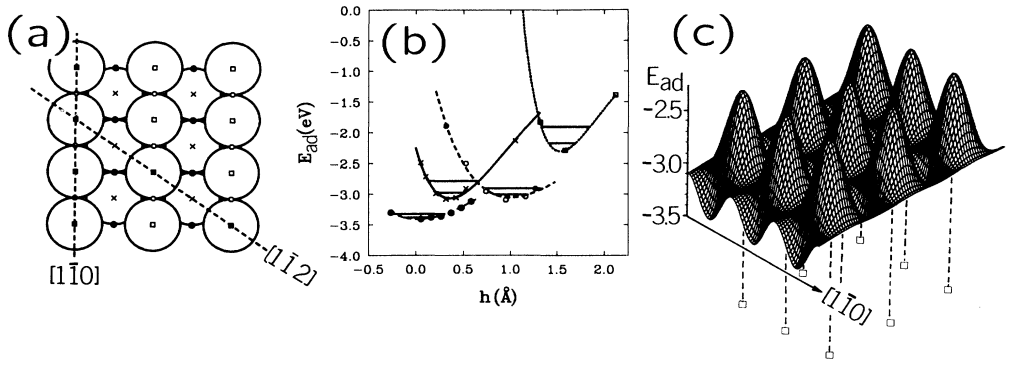

FIG. 10. (a) Schematic top view of Pd(110) and the assignment of adsorption sites: hollow (×), long bridge (•), short bridge (○), and on top (□). (b) H adsorption energy $E_{\rm ad}$ on Pd(110) as a function of the adsorption height h. The lowest two vibration levels are indicated in the potential wells. (c) Potential-energy surface $E_{\rm ad}$ for H/Pd(110) as a function of the hydrogen position in the surface plane, presented as a $3d$ plot. The position of Pd atoms is indicated by □ in (c).

TABLE II. Calculated values of the adsorption bond energy E_{ad}, adsorption height h_0, and vibration frequency ω for H on Pd(110).

Adsorption site	Coverage Θ	E_{ad} (eV) Calc.	h_0 (Å) Calc.	ω (meV) Calc.
Long bridge	1.0	−3.41	0.05	57
Hollow	1.0	−3.07	0.35	189
Short bridge	1.0	−3.05	1.0	100
On top	1.0	−2.30	1.53	263

gen in the (energetically) unstable on-top site would increase the surface energy.

Our results for the adsorption energies, summarized in Table II, establish that at low coverages, $\Theta < 1$, hydrogen occupies preferentially the trough sites, in agreement with experimental data obtained by LEED and LEIS.[14,15] Similar preferential adsorption sites have previously been found using the embedded-atom[26] and

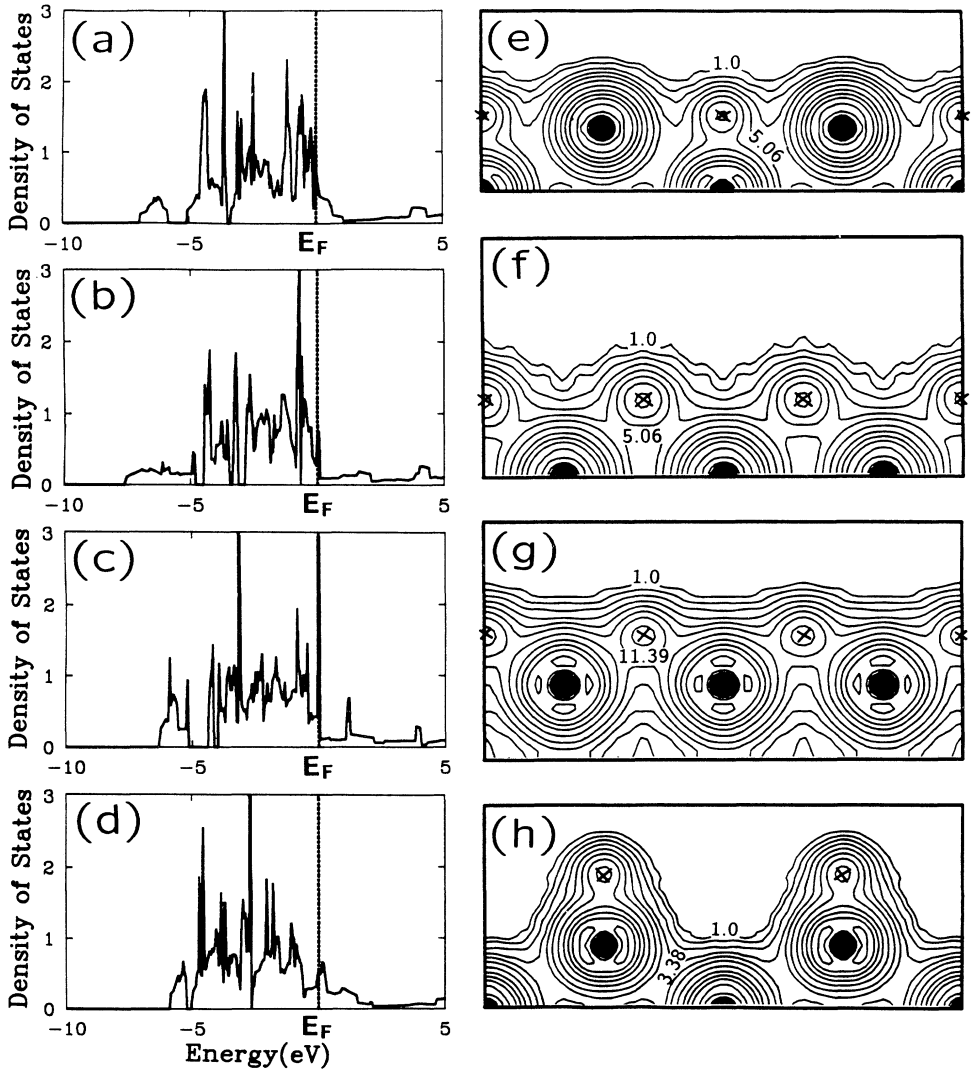

FIG. 11. Surface (slab-averaged) electronic density of states $N(E)$ for H/Pd(110) in (a) the hollow, (b) long-bridge, (c) short-bridge, and (d) on-top site. Charge density $\rho(\mathbf{r})$ for H/Pd(110) in (e) the hollow, (f) long-bridge, (g) short-bridge, and (h) on-top site. The contour plots (e) and (h) are shown in the $(\bar{1}11)$ plane (which contains the $[1\bar{1}2]$ direction) and the plots (f) and (g) are given in the (001) plane (which contains the surface $[1\bar{1}0]$ direction). The position of Pd atoms is marked by • and that of H atoms by ×. The charge density is in units of 10^{-2} e/a.u.^{3}; the ratio of two consecutive contours is $\rho(n+1)/\rho(n)=1.5$.

embedded-cluster[27] method. At higher coverages, $\Theta > 1$, new adsorption sites are occupied. Eventually, at large coverages exceeding $\Theta \approx 1.5$, a transition to a streaky (1×2) phase involving substrate reconstruction has been observed.[21,22]

Based on a careful analysis of LEED (Ref. 14) and He diffraction[16] data, the quasithreefold site [located in troughs between the hollow and the short-bridge sites shown in Fig. 10(a)] has been suggested as the preferential adsorption site for H in the (2×1) phase observed at low coverages $\Theta < 1$. Due to similarities in the chemical environment, we expect the nature of the H—Pd bond in the quasithreefold site to be very similar to the more symmetric bridge and hollow sites. We have performed no calculations for the quasithreefold site since the computational requirements for this low-symmetry site are very high.

Our equilibrium adsorption geometries are consistent with a H—Pd bond length of 2.0 Å in the twofold coordinated long-bridge and short-bridge sites. This is in excellent agreement with LEED results[14] for the H—Pd nearest-neighbor distance of 2.0±0.1 Å for H/Pd(110). For the singly coordinated on-top and hollow sites, the H—Pd bond length ranges between 1.5 and 1.7 Å, which is consistent with the sum of atomic radii of H and Pd.

At low hydrogen coverages $\Theta < 1$, two vibration modes have been observed[17,18] on Pd(110) single crystals at ≈100 and ≈120 meV. Assuming adsorption in the quasithreefold site of Pd(110), based on analogy to similar modes observed[60] for H/Pd(111), the higher-frequency mode has been assigned to a vibration perpendicular to the plane of the three Pd neighbors of H, and the lower mode to a motion parallel to this plane. While the calculation of these very-low-symmetry sites and the normal modes of H/Pd(110) is computationally too demanding, our values for ω in the chemically similar hollow and short-bridge sites, presented in Table II, lie in the same range as the experimental values. Our calculated value ω=57 meV for the long-bridge site seems to match perfectly with a low-frequency mode ω=58 meV, which has been observed on Pd powder and assigned to subsurface sites.[61]

As seen in Fig. 10(b), the hydrogen adsorption bond strength decreases in the sequence long-bridge → hollow → short-bridge → on-top site. In order to understand this trend, we show in Figs. 11(a)–11(c) the surface (slab-averaged) surface density of states $N(E)$ for the different adsorption sites. A comparison with the hydrogen-free Pd(110) surface density of states, given in Fig. 5(e), shows that the most prominent feature is a hydrogen-induced split-off state below the Pd 4*d* band, in close analogy with the hydrogen-covered Pd(001) surface [see Figs. 7(a)–7(d)]. In analogy with the Pd(001) results, we can correlate strong adsorption bonds with a large adsorbate-substrate hybridization in highly coordinated sites. This is supported by comparing the binding energies of the split-off state with respect to the bottom of the Pd band, which reflects the hybridization between palladium and hydrogen. Inspecting the densities of states, we find the binding energy of the split-off state to be largest in the long-bridge site and smallest in the on-top site.

In Figs. 11(e)–11(h) we present the total charge density of the H/Pd(110) system for the different adsorption sites for the equilibrium height h_0. The changing environment of the hydrogen atoms in the different adsorption sites modifies not only the depth, but also the shape of the H-Pd interaction potential, as shown in Fig. 10(b). As illustrated in Fig. 11(e) for the case of a hollow site, hydrogen prefers to be "buried" in the trough sites causing a smoothening of the surface charge density and a low vibration frequency. With decreasing coordination number, $E_{\rm ad}(h)$ resembles more a pairwise interaction potential that gives rise to an increasing vibration frequency ω [see the two lowest levels in Fig. 10(b)].

To establish the nature of the hydrogen-palladium surface bond, we determine the difference density of states $\Delta N(E) \equiv N_{\rm H/Pd(110)}(E) - N_{\rm Pd(110)}(E)$ and the charge-density difference $\Delta\rho \equiv \rho_{\rm H/Pd(110)} - \rho_{\rm Pd(110)} - \rho_{\rm H}$ for the hollow-site hydrogen. An inspection of the difference density of states for the hollow site, given in Fig. 12(a), shows that the main effect of hydrogen is to induce a split-off state below the bulk Pd band, and—to a lesser extent—modify the Pd 4*d* band. An analysis of the charge-density difference, given in Fig. 12(b), shows a charge transfer of ≈0.2 electrons towards hydrogen, stemming mainly from Pd atoms in the underlying layer. The nature of the H-Pd bonding mechanism can be seen from the charge density associated with the H-Pd split-

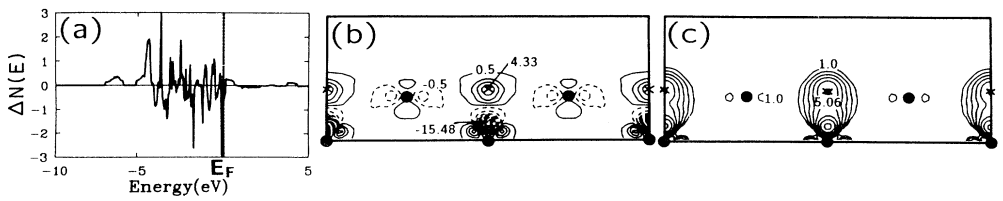

FIG. 12. (a) Difference density of states $\Delta N(E)$, (b) difference charge density $\Delta\rho(\mathbf{r})$, and (c) charge density associated with the H-induced split-off state [at $E \approx -7$ eV in Fig. 11(a)] for H/Pd(110) in the hollow site. The position of Pd atoms is marked by • and that of H atoms by ×. The charge density is in units of 10^{-2} e/a.u.^{3} In (b), the consecutive contours are separated by 10^{-2} e/a.u.^{3}, and in (c) the ratio of two consecutive contours is $\rho(n+1)/\rho(n)$=1.5.

off state at $\approx$ 7 eV below the Fermi level in Fig. 12(a), shown in Fig. 12(c). The covalent bonds result mainly from the hybridization of H 1*s* and Pd 4*d* states of second-layer substrate atoms neighboring the adsorbate. These states are very close in character to the H-induced split-off states in H/Pd(001), which are analyzed in Fig. 8.

VI. SUMMARY AND CONCLUSIONS

In summary, we used the *ab initio* pseudopotential local orbital method[34] to determine the interaction of hydrogen with the (001) and (110) surfaces of Pd as well as bulk Pd. Our calculations for the the H-Pd system have been completed by calculations for the H_2 molecule, the bulk, and the clean (001), and (110) surfaces of Pd.

We found that the preferential adsorption sites for hydrogen are the trough sites on Pd(110) and the fourfold hollow site on Pd(001) which corresponds to the octahedral site in bulk Pd. The formation of a H—Pd bond is accompanied by a transfer of $\approx$0.2 electrons from Pd to hydrogen. The signature of the H—Pd bond, which has a covalent H 1*s*–Pd 4*d* character and involves only the nearest neighbors of the hydrogen atom, is a split-off state located a few eV below the lower Pd 4*d* band edge. The presence of hydrogen in the bulk and at the surface of Pd causes a shift of the Pd 4*d* band to higher binding energies. For a nearly full 4*d* band, this increased band filling results in decohesion and softer force constants both at the surface and in the bulk. The calculated and observed lattice constant increase of $\approx$6% in bulk Pd upon hydrogen uptake in the high-density phase corresponds to a small hydrogen-induced expansion of otherwise slightly contracted Pd surfaces. In line with the general trend observed in chemisorption systems, lower-coordinated adsorption sites are energetically less favorable for hydrogen. With decreasing coordination number, the H—Pd bond length decreases from $\approx$2.0 to $\approx$1.5 Å and the H-Pd interaction potential becomes narrower, thus resulting in higher vibration frequencies.

ACKNOWLEDGMENTS

We thank Dr. C.T. Chan, Dr. M.A. Van Hove, Dr. S. Fahy, and Dr. M. Hybertsen for useful discussions and helpful comments. This work has been supported by the Office of Naval Research under Contract No. N00014-90-J-1396 and, in its initial stage, by the Director, Office of Energy Research, Office of Basic Sciences, Materials Sciences Division of the U.S. Department of Energy under Contract No. DE-AC03-76SF00098. CRAY computer time at the National Magnetic Fusion Energy Computer Center and the National Center for Supercomputing Applications and CONVEX computer time have been provided by grants from the U.S. Department of Energy, the National Science Foundation, and Michigan State University, respectively.

[1] *Hydrogen in Metals I and II*, Vols. 28 and 29 of *Topics in Applied Physics*, edited by G. Alefeld and J. Völkl (Springer-Verlag, Berlin, 1978).

[2] *The Chemical Physics of Solid Surfaces and Heterogeneous Catalysis*, edited by D.A. King and D.P. Woodruff (Elsevier, Amsterdam, 1982).

[3] *Hydrogen Damage*, edited by C.D. Beachem (American Society for Metals, Metals Park, Ohio, 1977); *Atomistic of Fracture*, Vol. 5 of *NATO Conference Series VI: Materials Science*, edited by R.M. Latanision and J.R. Pickens (Plenum, New York, 1983).

[4] J.F. Ziegler, T.H. Zabel, J.J. Cuomo, V.A. Brucic, G.S. Cargill III, E.J. O'Sullivan, and A.D. Marwick, Phys. Rev. Lett. **62**, 2929 (1989).

[5] Z. Sun and D. Tománek, Phys. Rev. Lett. **63**, 59 (1989).

[6] M. Fleischmann and S. Pons, J. Electroanal. Chem. **261**, 301 (1989); S.E. Jones, E.P. Palmer, J.B. Czirr, D.L. Decker, G.L. Jensen, J.M. Thorne, S.F. Taylor, and J. Rafelski, Nature (London) **338**, 737 (1989).

[7] M.G. Cattania, K. Christmann, V. Penka, and G. Ertl, Gazz. Chim. Ital. **113**, 433 (1983).

[8] R.J. Behm, K.Christmann, and G. Ertl, Surf. Sci. **99**, 320 (1980).

[9] K.H. Rieder and W. Stocker, Surf. Sci. **148**, 139 (1984).

[10] B. Tardy and J.C. Bertolini, C.R. Acad. Sci., Ser. 2 **302**, 813 (1986).

[11] C. Nyberg and C.G. Tengstål, Phys. Rev. Lett. **50**, 1680 (1983)

[12] F. Besenbacher, I. Stensgaard, and K. Mortensen, Surf. Sci. **191**, 288 (1987).

[13] D. Tománek, S.G. Louie, and C.T. Chan, Phys. Rev. Lett. **57**, 2594 (1986).

[14] M. Skottke, R.J. Behm, G. Ertl, V. Penka, and W. Moritz, J. Chem. Phys. **87**, 6191 (1987).

[15] R. Bastasz, T.E. Felter, and W.P. Ellis, Phys. Rev. Lett. **63**, 558 (1989).

[16] M. Baumberger, W. Stocker, and K.H. Rieder, Appl. Phys. A **41**, 151 (1986); K.H. Rieder, M. Baumberger, and W. Stocker, Phys. Rev. Lett. **51**, 1799 (1983).

[17] T.H. Ellis and M. Morin, Surf. Sci. **216**, L351 (1989).

[18] M. Jo, Y. Kuwahara, M. Onchi, and M. Nishijima, Solid State Commun. **55**, 639 (1985).

[19] H. Conrad, G. Ertl, and E.E. Latta, Surf. Sci. **41**, 435 (1974); M.G. Cattania, V. Penka, R.J. Behm, K. Christmann, and G. Ertl, *ibid.* **126**, 382 (1983); R.J. Behm, V. Penka, M.G. Cattania, K. Christmann, and G. Ertl, J. Chem. Phys. **78**, 7486 (1983).

[20] U. Memmert, J.-W. He, K. Griffiths, W.N. Lennard, P.R. Norton, N.V. Richardson, T.E. Jackman, and W.N. Unertl, J. Vac. Sci. Technol. A **7**, 2152 (1989); J.-W. He, D.A. Harrington, K. Griffiths and P.R. Norton, Surf. Sci. **198**, 413 (1988); J.-W. He and P.R. Norton, *ibid.* **195**, L199 (1988).

[21] G. Kleinle, M. Skottke, V. Penka, G. Ertl, R.J. Behm, and W. Moritz, Surf. Sci. **189/190**, 177 (1987).

[22] H. Niehus, Ch. Hiller, and G. Comsa, Surf. Sci. **173**, L599 (1986).

[23] K. Christmann, Z. Phys. Chem. Neue Folge **154**, 145

(1987).
[24] N.A. Baykara, J. Andzelm, D.R. Salahub, and S.Z. Baykara, Int. J. Quantum Chem. **29**, 1025 (1986); G. Pacchioni and J. Koutecký, in *Quantum Chemistry: Challenge and Transition in Metals Coordination Chemistry,* Vol. 176 of *NATO Advanced Study Institute Series C: Mathematical and Physical Science* (Kluwer, Dordrecht, 1986), p. 465.
[25] T.L. Einstein, M.S. Daw, and S.M. Foiles, Surf. Sci. **227**, 114 (1990).
[26] M.S. Daw and M.I. Baskes, Phys. Rev. B **29**, 6443 (1984).
[27] J.P. Muscat, Phys. Rev. B **34**, 8863 (1986).
[28] P. Nordlander and S. Holmström, Surf. Sci. **159**, 443 (1985).
[29] A. Haroun, L. Stauffer, H. Dreyssé, and R. Riedinger, Phys. Rev. B **38**, 12 150 (1988); L. Stauffer, R. Riedinger, and H. Dreyssé, Surf. Sci. **238**, 83 (1990).
[30] C. Umrigar and J.W. Wilkins, Phys. Rev. Lett. **54**, 1551 (1985).
[31] R. Biswas and D.R. Hamann, Phys. Rev. Lett. **56**, 2291 (1986).
[32] M. Weinert, A.J. Freeman, and S. Onishi, Phys. Rev. Lett. **56**, 2295 (1986).
[33] D.R. Hamann and P.J. Feibelman, Phys. Rev. B **37**, 3847 (1988).
[34] C.T. Chan, D. Vanderbilt, and S.G. Louie, Phys. Rev. B **33**, 2455 (1986); C.T. Chan, D. Vanderbilt, S.G. Louie, and J.R. Chelikowsky, *ibid.* **33**, 7941 (1986).
[35] W. Kohn and L.J. Sham, Phys. Rev. **140**, A1133 (1965).
[36] D.R. Hamann, M. Schlüter, and C. Chiang, Phys. Rev. Lett. **43**, 1494 (1979).
[37] L. Hedin and B.J. Lundqvist, J. Phys. C **4**, 2064 (1971).
[38] D.J. Chadi and M.L. Cohen, Phys. Rev. B **8**, 5747 (1973).
[39] B. Stoicheff, Can. J. Phys. **35**, 730 (1957).
[40] D_e denotes the depth of the H-H potential well rather than the observable dissociation energy from the vibrational and rotational ground state.
[41] This apparent underbinding, which is contrary to the usual LDA results, is partly due to the large spin-polarization energy of the isolated hydrogen atom and partly due to interactions between hydrogen atoms in the supercells.
[42] H. Chen, N.E. Brener, and J. Callaway, Phys. Rev. B **40**, 1443 (1989), and references cited therein.
[43] Ch. Kittel, *Introduction to Solid State Physics*, 6th ed. (Wiley, New York, 1986).
[44] H. Peisl, in Ref. 1, pp. 69 and 70.
[45] $E_{\rm coh}^{\rm expt}$(PdH) = −6.65 eV can be obtained from a thermodynamic cycle as a sum of the formation energy of PdH (from bulk Pd and *atomic* H), −2.76 eV per H atom, and the bulk cohesive energy of Pd, −3.89 eV per atom.
[46] P.K. Lam and R. Yu, Phys. Rev. Lett. **63**, 1895 (1989); X.W. Wang, S.G. Louie, and M.L. Cohen, Phys. Rev. B **40**, 5822 (1989).
[47] C.T. Chan and S.G. Louie, Phys. Rev. B **27**, 3325 (1983), and references cited therein.
[48] P.E.C. Franken, R. Bouwman, B.E. Nieuwenhuys, and W.H.M. Sachtler, Thin Solid Films **20**, 243 (1974); J. Hölzl and F.K. Schulte, in *Solid Surface Physics*, Vol. 85 of *Springer Tracts in Modern Physics*, edited by G. Höhler (Springer-Verlag, Berlin, 1979), p. 92.
[49] In the Pd(110) slab calculation, we have been using a less adequate basis set (which has *not* been augmented by floating orbitals due to the more complex geometry). Since floating orbitals affect the total energy more at the surface than in the bulk, the net effect is an underbinding of the slab. Secondly, the surface energy decreases if relaxations are considered.
[50] D. Tománek, S. Mukherjee, and K.H. Bennemann, Phys. Rev. B **28**, 665 (1983); **29**, 1076(E) (1984).
[51] A.R. Miedema and J.W.F. Dorleijn, Surf. Sci. **95**, 447 (1980).
[52] K. Binder and D.P. Landau, Surf. Sci. **108**, 503 (1981).
[53] We obtain $E_{\rm ad}$ at other than the calculated high-symmetry sites from a Fourier expansion over the reciprocal lattice. We keep only the lowest components of this expansion and determine the expansion coefficients from the calculated values for the high-symmetry sites.
[54] A.G. Egiluz, D.A. Campbell, A.A. Maradudin, and R.F. Wallis, Phys. Rev. B **30**, 5449 (1984).
[55] W. Drechsel, A. Murani, D. Tocchetti, W. Kley, I. Sosnowska, and D.K. Ross, J. Phys. Chem. Solids **37**, 1135 (1976).
[56] P.J. Feibelman and D.R. Hamann, Surf. Sci **179**, 153 (1987).
[57] K.P. Bohnen, Th. Rodach, and K.M. Ho, in The Structure of Surfaces III, edited by M.A. Van Hove, K. Takanayagi, and X. Xide (Springer-Verlag, Heidelberg, in press), and references cited therein.
[58] Our calculated value $\Delta d_{13} = -2.0\%$, which considers the interaction between the topmost and the third layer, lies close to the calculated value $\Delta d_{13} = -2.1\%$ for the Ag(110) surface (Ref. 57).
[59] Y. Cao and E.H. Conrad, Phys. Rev. Lett. **64**, 447 (1990).
[60] H. Conrad, M.E. Kordesch, R. Scala, and W. Stenzel, J. Electron Spectrosc. Relat. Phenom. **38**, 289 (1986).
[61] J.M. Nicol, J.J. Rush, and R.D. Kelley, Phys. Rev. B **36**, 9315 (1987); Surf. Sci. **197**, 67 (1988).